Journal of Applied Sciences

ISSN 1812-5654

science alert

ANSInet
an open access publisher
http://ansinet.com

Journal of Applied Sciences 8 (24): 4500-4511, 2008
ISSN 1812-5654

3D Point Wise Tracking of the Left Ventricle over Cardiac Image Sequences Using Active Mesh and Physical Models

[1]S. Kermani, [1]M.H. Moradi, [2]H. Abrishami-Moghaddam, [3]H. Saneei and [4]M.J. Marashi-Shoshtari
[1]Department of Bioelectrics, Faculty of Biomedical Engineering,
Amirkabir University of Technology, 424 Hafez Ave, Tehran 15875-4413, Iran
[2]Department of Electrical Engineering, K.N. Toosi University of Technology, Tehran 16315-1355, Iran
[3]Department of Internal Medicine, Isfahan University of Medical Sciences, Isfahan, Iran
[4]Department of Radiology, Isfahan University of Medical Sciences, Isfahan, Iran

Abstract: This study presents a strategy for point wise tracking of the Left Ventricle (LV) and recovering its motion field by 3D Active Mesh Model (AMM) and also continuum mechanics over 3D anatomical cine cardiac magnetic resonance imaging. The method is developed in the framework of the on-going work on application of mathematical modeling to image sequence analysis of cardiac wall as a non-rigid object. The model is composed of topology and geometry of LV and associated elastic material properties. The initial model acquires its knowledge directly from the 3D images in end diastolic phase. The LV deformation is estimated by fitting the model to the initial sparse displacement which is measured from a new establishing point correspondence procedure. The proposed approach is capable of estimating the displacement field for every desired points of myocardial wall, then it leads to measure dense motion field and local dynamic parameters such as Lagrangian strain. In this study, eight image sequences (including six real and two synthetic sets) were used and findings were in good agreement with those reported by other researchers. For synthetic image sequence sets, the mean square error between length of motion field estimated by the algorithm and analytical values was less than 1 mm. The results demonstrated the superiority of the novel strategy with respect to formerly presented algorithm mentioned in this study. This algorithm is more accurate while the running time has been reduced to one third. Furthermore, the results are comparable to the current state-of-the-art methods.

Key words: Cardiac MRI, deformable model, non-rigid motion, three dimensional active mesh model (3D-AMM)

INTRODUCTION

Regional dynamic characterization of the heart wall motion is necessary to isolate the severity and extent of diseases. With the increasingly wider availability of electrocardiographic (ECG)-gated tomographic image sequences, there have been many efforts on image-based analysis of the global and local motion of the heart, especially LV (Duncan and Ayache, 2000). The specificity of current various cardiac imaging modalities does not allow using conventional techniques such as block-matching or optical flow for motion study with proper precision. The goal of most research efforts has been to reliably recover the dense motion fields from a relatively unconfident sparse set of corresponding feature points. The recovery of the dense field motion and deformation parameters for the entire myocardium from the sparse set of displacements/veolcities is an ill-posed problem which needs additional constraints to obtain a unique solution in some optimal sense. Various strategies have been proposed over the past ten years with varying degrees of success, including notable examples of mathematically motivated regularization (Young *et al*., 1995; McEachen and Duncan, 1997; Shi *et al*., 2000), Finite-Element Method (FEM) based modal analysis (Benayoun and Ayache, 1998; Pham *et al*., 2001), spatiotemporal B-Spline (Huang *et al*., 1999), Fisher estimator with smoothness and incompressibility assumptions (Denney and Prince, 1995), statistical model (Lötjönen *et al*., 2004; Rueckert *et al*., 2003), deformable superquadrics (Bardinet *et al*., 1996), continuum biomechanics based energy minimization (Shi *et al*., 1999; Papademetris *et al*., 2001, 2002) and deformable model (Park *et al*., 1996; Bistoquet *et al*., 2007).

Continuum mechanical models have been used to regularize ill-posed problems in many applications in medical image analysis and also for cardiac wall motion tracking. The elastic model is designed to reduce bias in deformation estimation and to allow the imposition of proper priors on deformation estimation problems that

Corresponding Author: Mohammad Hassan Moradi, Department of Bioelectrics, Faculty of Biomedical Engineering, Amirkabir University of Technology, 424 Hafez Ave, Tehran 15875-4413, Iran
Tel: +98 21 6454 2399 Fax: +98 21 6646 8186

contain information regarding both the expected magnitude and variability of the deformation to be estimated. The myocardium is modeled using an elastic volumetric model in terms of hexahedral elements for applying continuum mechanical constraints (Shi *et al*., 2000; Papademetris *et al*., 2002). Their measurements and models are integrated within a Bayesian estimation framework. Pham *et al*. (2001) proposed an iterative procedure on an active region model that deforms and pulls towards the image edges using the finite element method. Among the large collection of existing segmentation algorithms (Frangi *et al*., 2001), approaches based on deformable surface have been extensively studied. They show the relevance of deformable model approaches for LV segmentation due to their ability to introduce prior knowledge. Deformable models are also well suited for the image analysis task (McInerney and Terzopoulos, 1996; Montagnat *et al*., 2001, 2005). Recently, an incompressible model was presented for recovering the LV deformation (Bistoquet *et al*., 2007). The mathematical foundations of deformable models represent the confluence of geometry, physics and approximation theory. Geometry serves to represent object shape, physics imposes constraints on how the shape may vary over space and time and optimal approximation theory provides the formal underpinnings of mechanisms for fitting the models to measured data (McInerney and Terzopoulos, 1996). Among these models, AMM permits a large number of degrees of freedom to the object (Montagnat *et al*., 2001). It has the ability to merge continuum mechanical constraints and many rules in cardiac wall motions. The AMM-based tracking methods previously introduced were presented in 2D space (Lautissier *et al*., 2003). Algorithms for point-wise tracking and analysis of cardiac motion based on 3D-AMM were presented previously (Jamali-Dinan *et al*., 2007). In this study, first the 3D epi/endocardial surfaces were extracted from the End Systole (ES) frame. LV was modeled as an elastic wall in a motionless large elastic cube for applying continuum mechanical constraints. For mesh initialization, these surfaces were fed to a 3D Delaunay triangulation and then to a tetrahedralization algorithm. The mesh which was constructed using this method places more tetrahedra over high detailed areas. An estimation of the object deformation is achieved based on a set of sparse initial displacement measurements as a result of a robust least square technique. This estimation is then used by the tracking algorithm for measuring the local deformation parameters of the 3D object. However, there are some shortcomings in this approach which are addressed here.

First, the study on elements which is created by Refined Constrained Delaunay Tetrahedralization (RCDT) algorithm (Si, 2006) showed that approximately 40% of elements between epicardial and endocardial wall. The remaining 60% elements have nodes that placed outside of the left ventricular wall and can not be tracked so this will impose high calculation costs to solve the problem. The cost will intensively increase when the number of elements increases. For example, the calculation time for an image sequence with a single change in reference frame from ES to End Diastole (ED) is presented in Table 1. The cost is 6.5 times higher for a 2.3 times increase in the number of nodes. Due to such limitations, former implementation was made on (50%) reduced spatiotemporal resolutions. In other words, half of the data had to be ignored causing a considerable amount of error.

Table 1: Running time and meshing configuration for two reference frame: ES, ED in our pervious work

	Running time (s)	No of elements	No of nodes
Ref: ED	22412	12871	1144
Ref: ES	3447	8353	493
Ratio	6.50	1.54	2.30

Second, in the stage of tracking the points on the surfaces from one frame to the next, the points are not put in correspondence confidently, thus determination of correspondent points shows various confidence measures. Applying these points with identical weight in least square estimation causes various errors. This study presented a new approach to overcome these limitations and improve our previous works (Jamali-Dinan *et al*., 2007). This study made the following contributions:

- Evaluating the performance of the proposed algorithm using comprehensive experiments on synthetic (Arts *et al*., 1996) and real cardiac MRI datasets
- Many researchers used prior assumptions about model such as a cube includes LV surfaces (Jamali-Dinan *et al*., 2007), a half ellipsoid shell (Pham *et al*., 2001), balloons (McInerney and Terzopoulas, 1996), superquadric (Bardinet *et al*., 1996), a pseudo thin plate splines on the sphere at end-diastole (Bistoquet *et al*., 2007). In this study, 3D-AMM was initialized directly from the 3D image in ED frame of the cardiac cycle
- Improving the algorithm efficiency by optimizing the number of mesh elements and applying a volumic template which covers only LV muscle
- Capability of estimating the displacement field from all points on LV wall or in the myocardium and color kinesis evaluation of LV
- Fitting 3D-AMM to initial sparse displacements with considering to their confidence
- For establishing the correspondence points, a robust restricted block matching algorithm was proposed based on weighted-correlation
- Applying different mechanical specification properties of the heart tissue during entire cardiac cycle

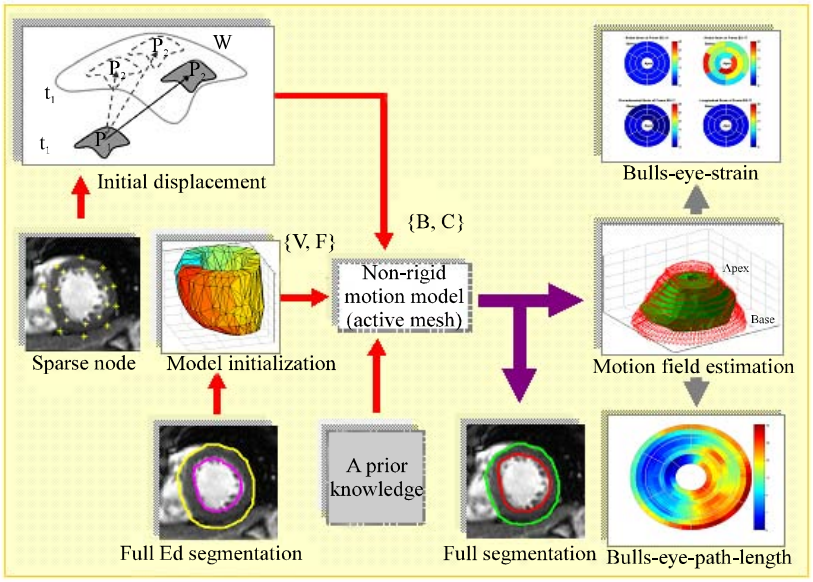

Fig. 1: The block diagram of the full analysis scheme

MATERIALS AND METHODS

Figure 1 shows a block diagram of the full analysis scheme presented in this study. After preprocessing and segmentation of LV, the epi/endocardial surfaces in ED frame are fed to creating a template as a model initialization. Establishing correspondence of the points is performed considering the contouring data. For each pair of correspondent points a confidence measure is determined. The description of 3D-AMM, fitting 3D-AMM to the initial sparse displacements with considering their confidence and usage of a priori information of cardiac wall motion phasing is stated in Non-rigid motion model. The whole procedure of the algorithm consists of the following steps:

Step 1: Both ES and ED frames and also regions of interest in all images are selected by the user

Step 2: In ED frame, epicardial and endocardial contours are determined by LV segmentation, then generate a volumic template

Step 3: The template is represented by the refinement of constrained Delaunay tetrahedra (Si, 2006).

Step 4: Cubic spline interpolation is used to convert the voxels to cubic elements for point correspondence procedure

Step 5: The mechanical specification model of the heart tissue is different in contraction and relaxation. The epi/endocardial contour data together with image data set are interpolated and the reference template is partitioned in order to make the dense field estimation possible by enforcing appropriate mechanical properties for each frame which results in a higher performance regularization

Segmentation of LV in CMRI image sequences: All slices are segmented interactively based on the algorithm introduced by Heiberg *et al.* (2005) in all frames. This method is also based on the concept of deformable models, but extended with an enhanced and fast edge detection scheme that includes temporal information and anatomical a priori knowledge. The LV model used in this approach is a time-resolved mesh representation of LV as an open cone, sliced along its long axis with an equal number of points for each slice. The number of points for each slice contour is selected to be 80. Toward a fully 3D cardiac wall motion analysis, we will merge the level set procedure (Jamali Dinani *et al.*, 2007) to our proposed algorithm.

Model initialization: We made a volumic template from the 3D image which covers LV muscles environmentally and then tetrahedralized it by RCDT. The proposed model-building method does not depend on prior assumptions about the 3D scene structure; instead it attempts to accumulate this knowledge directly from the images. The mesh generated from the Delaunay tetrahedralization of a general point set is not only a good mesh, but also a unique one and optimized in size and the number of elements. In addition, the mesh which was constructed using this method places more tetrahedra over high detailed areas. Therefore, we use its geometrical representation to describe the template. The procedure of creating template comprises the following steps:

- Creating new contours from segmentation results according to the Eq. 1:

$$X_{Tem} = \begin{cases} X + \text{sgn}(X_C - X) & X \in \text{Endocardial surface} \\ X - \text{sgn}(X_C - X) & X \in \text{Epicardial surface} \end{cases} \quad (1)$$

where, X_C is the endo/epicardial centeroid of its slice, X = [x, y, z] is the coordinate point which belongs to endo/epicardial layer and X_{Tem} is the respected template point.

- Smoothing the contours by Non-shrinkage Gaussian filter (Shi *et al*., 2000)
- 3D Delaunay triangularization is applied for geometrical representation of LV surfaces
- Creating a general point set to satisfy both non-collinearity and non-cosphericity assumptions from represented LV surfaces (previous step)
- Using geometrical representation of the template by RCDT

The great advantage of the template is the tangent covering of the whole LV muscle then all edge points are in the template. Thus, the displacement vectors of each point, on LV wall or in the myocardium, can be estimated by the linear interpolation of the tetrahedral element node coordinates over the entire cycle.

Obtaining initial sparse displacement data: For establishing the correspondence points on epicardial and endocardial contours, a robust restricted block matching algorithm was proposed based on weighted-correlation. We do this weighted correlation-based search only for selected points that are on the edge of the 3D epi/endocardial in the next frame which have the opportunity to correspond to their previous sparse frame point. According to the motion limitation, this selection is based on points located in the same spatial sector. The point correspondence procedure details of this point set can be described by the follow:

- Calculating the 3D gradient of the selected point in current frame by Sobel operator
- Determining the discrete gradient direction. There are 13 gradient directions in the discrete 3D image; the 3D space around each point is divided into 13 volumetric sectors. Therefore, a 3×3×3 mask is defined for each major direction which can be called direction mask
- For each point, its direction mask imposes to a 3×3×3 window centered at selected point due to edge enhancement and weighted-correlation in the next step
- We correlate the 3×3×3 window centered at the fiducial point in the current frame with 3×3×3 windows centered at the candidate points in the next frame. The centered point which its window gives the maximum normalized cross-correlation value is chosen as the correspondent point. Then displacement vector measurement (B_i) was estimated by the point and its correspondence
- The maximum normalized cross-correlation value is chosen as a confidence measure (C_i)

Non-rigid motion model (3D-AMM): Image deformations result from change in the geometrical view point and physical deformations of the object in the scene. In order to accurately represent these deformations, the 3D-AMM incorporating the geometrical and physical characteristics are defined in this research. We consider LV as a continuous elastic medium. It is submitted to external image forces that push the model's interfaces towards the image edges. 3D-AMM is a combination of:

- A topological and geometric model of the heart.
- A constitutive equation defining its dynamical behavior under applied external forces.

The equilibrium of the model is obtained when the following global energy functional is minimized:

$$E = E_{data} + E_{elastic} \quad (2)$$

where, E_{data} is the energy due to the external forces and $E_{elastic}$ represents the deformation energy of the model. The medium is considered as a linear elastic solid. The elastic energy can then be expressed as (Tirupathi *et al*., 2002):

$$E_{elastic} = \frac{1}{2}\int_{\Omega} \sigma^{t}\varepsilon \, d\Omega \quad \text{where } \sigma = K\varepsilon \quad (3)$$

For the sake of simplicity, the material is considered as transversely isotropic and completely defined by the Young modulus E and the Poisson's ratio v. Then, with the small displacement assumption ε = Su.

$$E_{elastic} = \frac{1}{2}\int_{\Omega} (Su)^{T} K (Su) d\Omega \quad (4)$$

where, S is a differential operator, K is the elasticity matrix and Ω is the space occupied by the LV muscles. Let T = {V, F} be a tetrahedralization defined over the template, where F is a set of tetrahedra and V is a set of their vertices. In the discrete form, the elastic energy $E_{elastic}$ is given by (5):

$$E_{elastic} = \frac{1}{2} U^{T} K U \quad U = \left[..dx_i..|..dy_i..|..dz_i..\right], \; i = 1, 2, ...M \quad (5)$$

Where, U is a vector of elementary deformation, M is the number of vertices and K is the stiffness matrix. The stiffness matrix should be assembled from elementary stiffness matrices associated with each tetrahedral element (Tirupathi *et al.*, 2002). The stiffness matrix is then given by (6):

$$K = \sum_{e \in f} K_e \text{, where } K_e = V_e B_e^T D B_e \quad e = 1 \cdots Elem \tag{6}$$

For eth element, K_e is the element stiffness matrix, V_e is its volume, B_e is a 6×12 matrix with elements defined by the coordination of its vertices. D is a 6×12 matrix defined by the material properties of the deforming body. The matrix D which proposed by Papademetris *et al.* (2002) is as follows (7):

$$D^{-1} = \begin{bmatrix} \frac{1}{E_p} & \frac{-v_p}{E_p} & \frac{-v_{fp}}{E_f} & 0 & 0 & 0 \\ \frac{-v_p}{E_p} & \frac{1}{E_p} & \frac{-v_{fp}}{E_f} & 0 & 0 & 0 \\ \frac{-v_{fp}E_f}{E_p} & \frac{-v_{fp}E_f}{E_p} & \frac{1}{E_f} & 0 & 0 & 0 \\ 0 & 0 & 0 & \frac{2(1+v_p)}{E_p} & 0 & 0 \\ 0 & 0 & 0 & 0 & \frac{1}{G_f} & 0 \\ 0 & 0 & 0 & 0 & 0 & \frac{1}{G_f} \end{bmatrix} \tag{7}$$

where, E_f is fiber stiffness, E_p is cross fiber stiffness, v_p, v_{fp} are the corresponding Poisson's ratios of them and G_f is the shear modulus across fiber ($G_f \approx E_f/(2(1+v_{fp}))$). The fiber stiffness was set to be 3.5 times greater than cross fiber stiffness. The fiber stiffness and Poisson's ratios are constants corresponding to the approximately incompressible properties (the typical values are $v_p = v_{fp} = 0.4$ $E_P = 100$). Then E_f and G_f were calculated.

E_{data}: Given a set of displacement vector measurements B and confidence measures C from previous stage. Thus the E_{data} is given by 8:

$$E_{data} = \sum_{i=1}^{N} \lambda_i^2 \left\| d_i - \delta_i \right\|^2 \text{ where } \delta_i = \left[\delta x_i, \delta y_i, \delta z_i \right] \text{and } i = 1, \ldots, N \tag{8}$$

d_i is the displacement vector which is obtained from the model and δ_i is the displacement vector which is obtained from the point correspondence procedure . N is the number of displacement vectors (N < M). λ_i is ith weighted factor. The importance of the ith term in the Edata is tuned by $\lambda_i^2 = C_i$ which is the confidence of ith

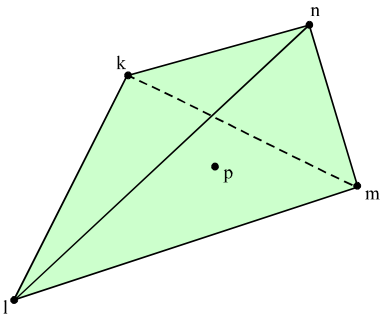

Fig. 2: A fiducial point (p) in the tetrahedron as used in Eq. (9)

displacement vector. In Fig. 2, at a point (P) in the tetrahedron $\Delta\, p_k\, p_l\, p_m\, p_n$, the deformation function d_i (x, y, z) is estimated by (9).:

$$\begin{aligned} d_i(x,y,z) = g_k(x,y,z)D_k + g_l(x,y,z)D_l + \\ g_m(x,y,z)D_m + g_n(x,y,z)D_n \end{aligned} \tag{9}$$

where, $D_i = (dx_i, dy_i, dz_i)$ the ith displacement vertex and g_i is the ratio volume of pyramid fiducial point P and other points except ith point to the volume of pyramid $\overset{\Delta}{klmn}$ that point P belongs to it. Then for the set of displacement vector measurements B, estimated $\hat{B}$ which obtained from the model is given by (10):

$$\hat{B} = AU \text{ where}$$

$$A = \begin{pmatrix} Q & 0 & 0 \\ 0 & Q & 0 \\ 0 & 0 & Q \end{pmatrix}_{3N \times 3M} \quad Q_{ij} = \begin{cases} g_j(x_i, y_i, z_i), \; j = \{k, l, m, n\} \\ \quad , (\hat{x}_i, \hat{y}_i, \hat{z}_i) \in \Delta P_k P_l P_m P_n \\ 0 \quad , \text{otherwise} \end{cases} \tag{10}$$

Fitting the model to data: For estimation of the model parameters, the displacement vectors of M vertex U, the global energy functional (2) is minimized (11):

$$\arg\min_U \left\{ \sum_{i=1}^{N} \lambda_i^2 \left\| d_i - d_i \right\|^2 + \lambda_G U^T K U \right\} \text{ where } i = 1, \ldots, N \tag{11}$$

λ_G is the global regularizing factor. The above minimization (11) is seen to be equivalent to the minimization (12):

$$\begin{aligned} &\min_U \left\{ \left\| \lambda AU - \lambda B \right\|^2 + \lambda_G U^T K U \right\} \\ &\text{where } B = \left[\ldots \delta x_i \ldots \middle| \ldots \delta y_i \ldots \middle| \ldots \delta z_i \ldots \right]^T \text{ and } \lambda = [\ldots \lambda_i \ldots], \; i = 1, \ldots N \end{aligned} \tag{12}$$

The solution of (12) is (13), which gives the displacement of all vertices of the mesh. Then, the displacement of all points of LV muscle will be obtained by linear interpolation (9). The equation (13) is solved by Moore_Penrosed inverse matrix (14) (Moore *et al.*, 2000):

$$\hat{U} = (\lambda A^T A + \lambda_G K)^{-1} \lambda A^T B \quad (13)$$

Estimation of path length and strain: It is shown that changes in motion parameters (path length and strain measures) between normal and injury regions are significantly different and indicate of the myocardial function. The variation of these parameters can be used to diagnose the location and extent of myocardial injury. This fact is validated using post mortem Triphenyl-Tetrazolium Chloride staining technique (Shi *et al*., 2000).

The path length of any myocardial point is the sum of the magnitudes of all displacement vectors of that point over the cardiac cycle and it measures the overall motion of the point. For estimation of displacement vectors of each point, on LV wall or in the myocardium, we used Eq. 9 over the entire cycle. According to the fact that the deformation of all tetrahedra in the template over the entire cardiac cycle is clarified by the model and each fiducial point (on LV wall or in the myocardium) belongs to one of the tetrahedral elements is due to definition of the template. Therefore, all of the displacement vectors of this point are clarified by Eq. 9 during the cycle.

Strain is a dimensionless quantity measuring the percent change in length at different points of a deforming continuous body. Lagrangian strain maps are produced from our model by describing the deformation of LV in the Lagrangian reference frame. The ED frame is considered as the reference frame. The dense displacement field is available from the model; hence the strain of deformation can be computed at each myocardial point. In the Lagrangian reference frame, the mapping $\Gamma(X)$ warps X into x then, The Lagrangian strain tensor is defined as:

$$E = \frac{1}{2}(C - I) \quad \text{and} \quad C = F^T F \quad (14)$$

where, C and F is the Cauchy-Green and gradient deformation tensors, respectively and I is the identity matrix. This can also be deducted directly from the definition in Eq. 15. Consequently, E can be expressed as:

$$E = \frac{1}{2}\left(F^T F - I\right) \text{ where } F_{ij} = \frac{\partial x_i}{\partial X_j} \; i, j = \{1,2,3\} \quad (15)$$

The quantity $M^T E M$ will give the value of the normal strain in the direction given by the unit vectors M. Due to the ventricular geometry, it is appropriate to calculate the myocardial strains based on the radial, circumferential and longitudinal directions.

Visualization of the result: At the conclusion of model fitting, a sequence of the T = {V, F} sets is obtained. In each frame, the LV wall is represented with a set of tetrahedra which have specific geometry and topology in the 3D space. So it is possible to obtain 2D and 3D visualizations that are combination of geometry, anatomy and local parameters such as strain and path length. By assembling tetrahedra /triangles, cardiac wall/surfaces can be produced during the cardiac cycle. Viewing these cardiac wall/surfaces in a cine-loop provides a good impression of the overall 4-D LV motion.

3D visualization: Figure 3 shows the extracted cardiac wall in six phase of cardiac cycle by assembling tetrahedra. We assumed that the local cardiac dynamic quantities in a tetrahedron can be constant due to little size of thetrahedra. It is possible to calculate the local quantities in the centroid of every tetrahedron and visualize the quantities with color coding.

Figure 4 is the presentation of radial, circumferential and longitudinal Lagrangian strain quantities in ED and ES phases. The 3D motion fields mapping is also shown in Fig. 5. It shows the ability of the proposed algorithm to generate 3D motion field. The 3D motion field in this figure is the difference between position vectors in ED and correspondence points in ES. This field is uniformly sparse due to limitation of the presentation.

2D visualization: For color kinesis evaluation of LV, a propounded way is the 2D visualization of the original anatomical data together with analyzed result in polar representation or bulls-eye. From the clinical point of view, this representation could be considered as an advantage considering that cardiologists are already familiar with "bulls-eye" maps that are often used for representing myocardial perfusion during nuclear medicine studies. The result of the regional parameters (strain or path length) can be visualized per slice as color

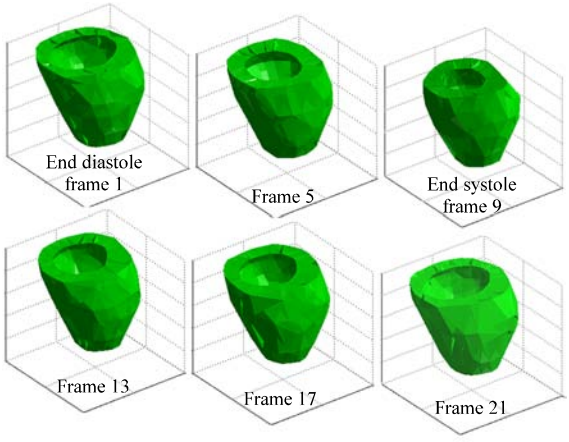

Fig. 3: Visualization of the LV wall motion results

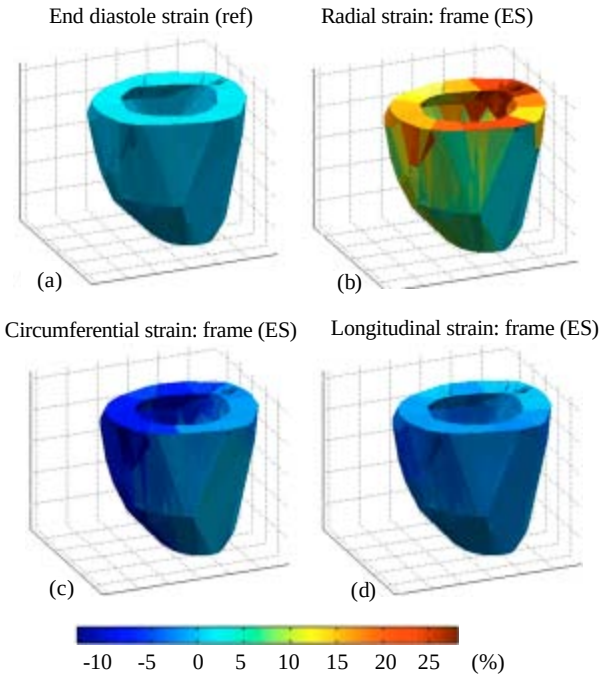

Fig. 4: The derived strains: (a) ED strain and (b-d): ES radial, circumferential and longitudinal strain, respectively

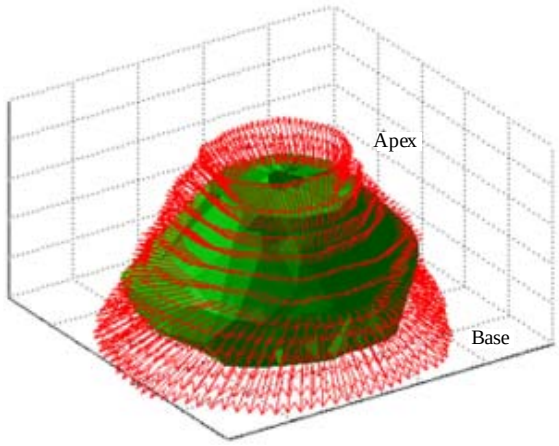

Fig. 5: 3D motion field with cardiac wall in ES

overlay on the original anatomical image data and for all slices together in a bulls-eye representation. This 2D mapping of path length with color map is shown in Fig. 6 and 11.

Consequently; the algorithm is capable of obtaining and visualizing the local parameters in all points of myocardium or LV surfaces such as path-length or strains and motion field.

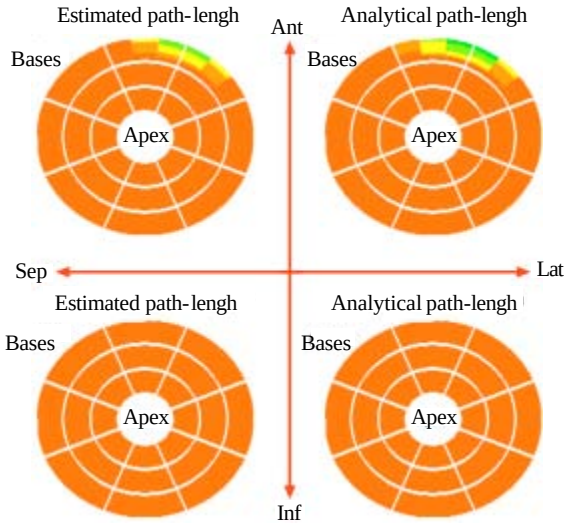

Fig. 6: Comparison between normalized analytical and estimated path-length: Bulls-eye; normal (down) and abnormal (up)

RESULTS

For evaluation of this proposed algorithm, we used eight image sequence sets, six real (five volunteers and a patient) and two synthetic groups. We reconstructed the deformation field within the myocardium over the entire cycle. For each set, strain and path-length computed from the proposed algorithm. For two synthetic sequence sets, the path-length were compared to those obtained from analytical model of CMRI simulator. Finally, the trajectories which were obtained from both estimated and analytical procedures were also compared.

Synthetic sequence CMRI: We used a computational simulator to generate two sets of Gradient Spine Echo synthetic image sequence. The simulator incorporates a parametric model of LV motion presented by Arts *et al.* (1992) and applying it to a confocal prolate spherical shell, resembling the shape of LV. Every point of this shell is displaced in the space due to the kinematic model of LV. The model is made to assume a configuration representing one of 60 phases in the cardiac cycle. We simulated a gradient-echo CMRI imaging sequence with intersecting the shell and the plane at a desired orientation. In the image, the gray level of each common point between the plane and shell was set to 100 (dark) and others to 255 (white). The inverse motion map is presented analytically, allowing point-wise correspondences to be made between points at any two frames. Then, there is the true 3D motion in the output so that the motion estimation

algorithm can be compared against the truth. In order to assess the robustness of the proposed method, we contaminated these images with normal distributed random noise in the determined level of SNR. Another imaging sequence was generated in similarly, but mechanical parameters are changed in the lateral basal region as a simulation of hypokinetic heart disease region. The motion in this center region was 75% of a normal zone. Assuming LV wall volume is constant and almost equal to 100 cm^3 and LV cavity volume changes from 60 to 120 cm^3 during a cardiac cycle. The specification of confocal prolate spherical shell model is as follows:

$$\begin{aligned} &x = \delta \sinh \lambda \sin \eta \cos \varphi \\ &y = \delta \sinh \lambda \sin \eta \sin \varphi \\ &z = \delta \cosh \lambda \cos \eta \\ &\text{where, } \delta = 5, \lambda: 0.4 \text{ to } 0.6 \\ &0 \le \eta \le 120 \quad 0 \le \varphi \le 360 \end{aligned} \tag{16}$$

The shell intersects with 64 parallel planes in equal distances. The result of this simulation was 64 2D images for each frame. The size of these images is 64×64 and their resolution is 1.1 mm in all directions. Then the size of the image sequence set of 64×64×60×64 is decreased to 64×64×15×12, as the standard CMRI sequence. Validation of the proposed method is estimated on these synthetic image sequences for which a ground truth about the LV volume is known. For this reason, the displacement of points on all contours are achieved from the analytical generator and estimated by the proposed method during an entire cardiac cycle. The mean square error is calculated by the Eq. 17. This procedure is repeated for the synthetic image sequences with different contaminated noise level and shown in Table 2.

$$MSEF_f = \frac{1}{NFram}\sqrt{\sum_{i=1}^{NNod}\left\|U_i^f - \hat{U}_i^f\right\|^2} \tag{17}$$

$$MSE = \frac{1}{NFram}\sum_{f=1}^{NFram} MSEF_f$$

where, $\hat{U}_i^f$ and U_i^f are the estimated and analytical displacement vector of ith node in the fth frame, respectively. ‖ ‖ is the norm of a vector. $MSEF_f$ is mean square errors in the fth frame. NFram and NNod are the number of frames and nodes, respectively. Table 2 compares the dense motion fields provided by algorithm with its analytical value and the result of Mean Square Error (MSE) value versus Signal to Noise Ratio (SNR). Figure 7 also demonstrates the MSE of motion field vs. frame, where the mean error value of all frames is 0.69±0.23 mm at 0 dB SNR. Thus, it seems that the proposed approach is robust. Despite the meshing object was refined, the running time of the algorithm was 1/3 of the previous algorithms (Jamali Dinani *et al*., 2007) due to the ability of the proposed model which eliminates nodes and elements outside the cardiac wall.

Table 2: Estimated dense motion fields compare with their Analytical fields

SNR	0	5	10	20
Mean error (%)	0.845	0.816	0.77	0.78
Running time (sec)	878	815	810	811

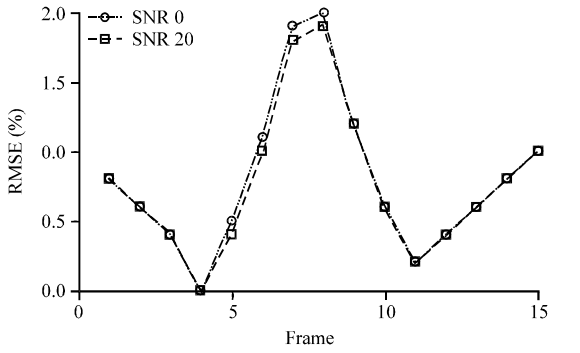

Fig. 7: Root mean square errors of motion fields versus frame, provided from synthetic image sequences in two SNR levels

For reporting purposes, the LV was divided into three slices, each consisting of eight sectors. Bulls-eye of normalized path-length estimated motion field (right) and the analytical values (Left) of two synthetic image sequences is shown in Fig. 6. The hypokinetic region completely detected and there are significant differences between the values of the base and hypokinetic area (yellow and green in basal ant. lateral and basal ant.). The extraction of motion field is also robust to noise.

Real sequence CMRI: The result of evaluation on six sets of Gradient-Echo images is given in this research. MR imaging was performed on a Symphony Siemens 1.5 Tesla scanner at Isfahan MRI center. Short-Axis (SA) images through LV were obtained with the turbo GSE cine technique, using the following parameters: TR = 42-44 ms, TE = 1.38-1.45 ms, FA = 53°, SL = 5 mm and resolution in plane 256×256. The protocol is called tf2d20-12Slices-shph-12bh. With this protocol, short breath-hold scans and multislice applications in one breath-hold are possible. The contrast is a function of T1/T2* and independent of TR. Table 3 are contain of the specification of the data sets.

The patient is a 67 year-old man with 70% stenosis of left anterior descending artery in the recent angiography and hypokinetic septum on echocardiography and also ECG evidence of myocardial infarction of septal wall. The MRI cardiac data of the patient is shown in Fig. 8.

Table 3: MRI specification of six real CMRI data sets

	Ag	SR	TR	Fr	Dis	Sl	TE	FOV
P1	65	0.98	44.94	21	0.25	12	1.45	25
V1	62	0.98	43.96	22	1.56	9	1.38	25
V2	50	0.78	43.2	16	1.25	9	1.5	20
V3	24	1.09	42.32	17	1.95	10	1.45	28
V4	45	0.98	44.24	19	1.56	10	1.38	25
V5	54	0.98	44.94	21	2	9	1.45	25

in the table SR: special resolution in mm, T.R: Temporal resolution in msec, Fr: the number of frame, Dist: Distance between two adjacent slices in mm, Sl: The number of slices, TE: Echo time in msec, FOV: Field of view in cm, P: Patient and V: Volunteer

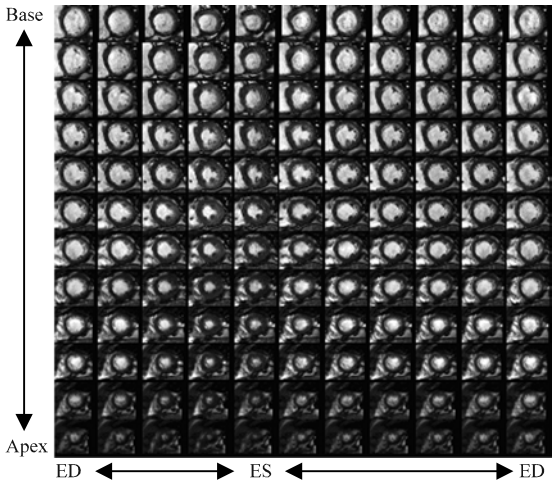

Fig. 8: The cardiac MRI data of the patient. The horizontal line consists of frames 1, 3, 5, 7, 9, 11, 13, 15, 17, 19 and 21 of each slice and 12 slices for the vertical line, base to apex

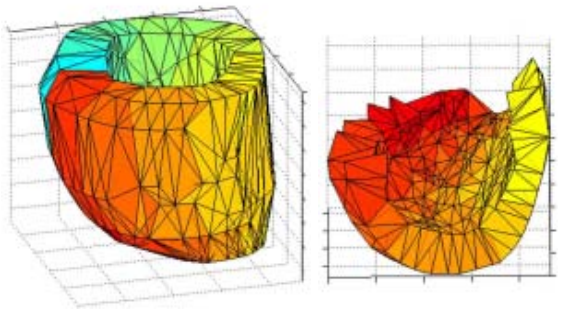

Fig. 9: The template of the LV wall for the ED phase of cardiac cycle

In these images, the region containing LV is selected; hence, the size of the image matrix is reduced to 109×86. Figure 9 illustrates the result of model initializing and tetrahedralizated template of LV wall. Figuer 10 also shows the result of mapping the trajectory of a set of points in 2D.

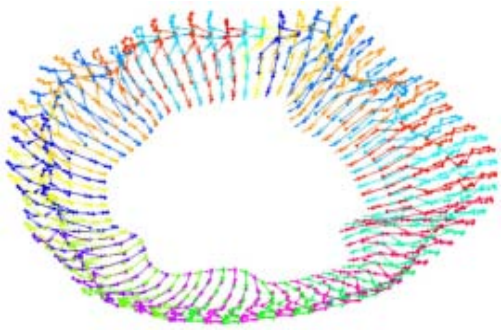

Fig. 10: The trajectory of a set of myocardial points mapped in 2D

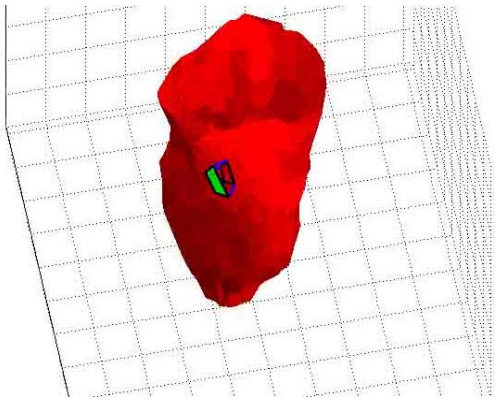

Fig. 11: Mapping of the endocardial surface: endocardial surface in ES phase is rendered light red

Figure 11 illustrates the LV endocardial surface of a normal subject in the ES phase with an embedded curvilinear quadrilateral. It shows that the quadrilateral is deformed to ED phase, by applying the derived transformer. It can also be seen that the curvilinear quadrilateral moved outward (radial expansion), downward (longitudinal shortening), rotated and slanted (circumferential twist). In Fig. 12, the path-length values visualized by bulls-eye, (a) is the path-length values of the patient's images analysis and (b) is the average values for five volunteers. In septal region, the path-length values in basal levels were 11-15 and 17-25 mm for the patient and the volunteers, respectively. This amount in apical levels was 6-10 and 16-22 mm for the patient and for the volunteers. Briefly, at a glance the hypokinesis of the septal region is significant when comparing both a and b. These results are consistent with the clinical evidence of the patient.

Figure 4 shows the estimated radial, longitudinal and circumferential strains which are in ES phase. It denotes that the behavior of strain in LV derived from normal

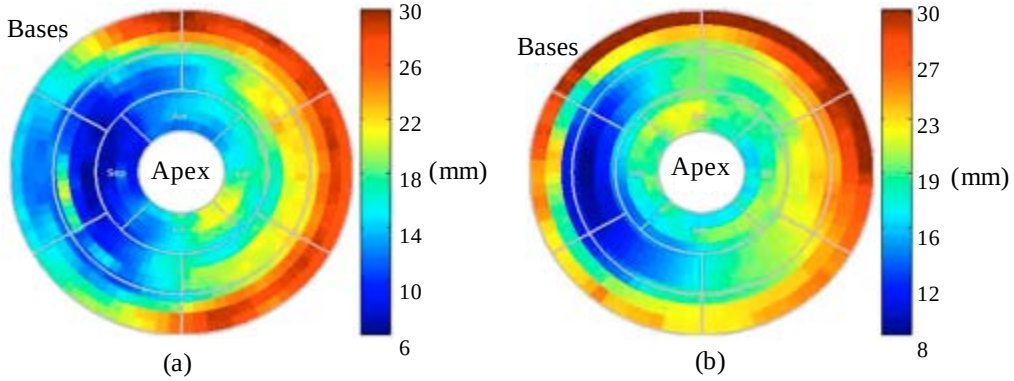

Fig. 12: Bulls-eye of path-length of myocardial point across two human data sets. (a): patient and (b): normal

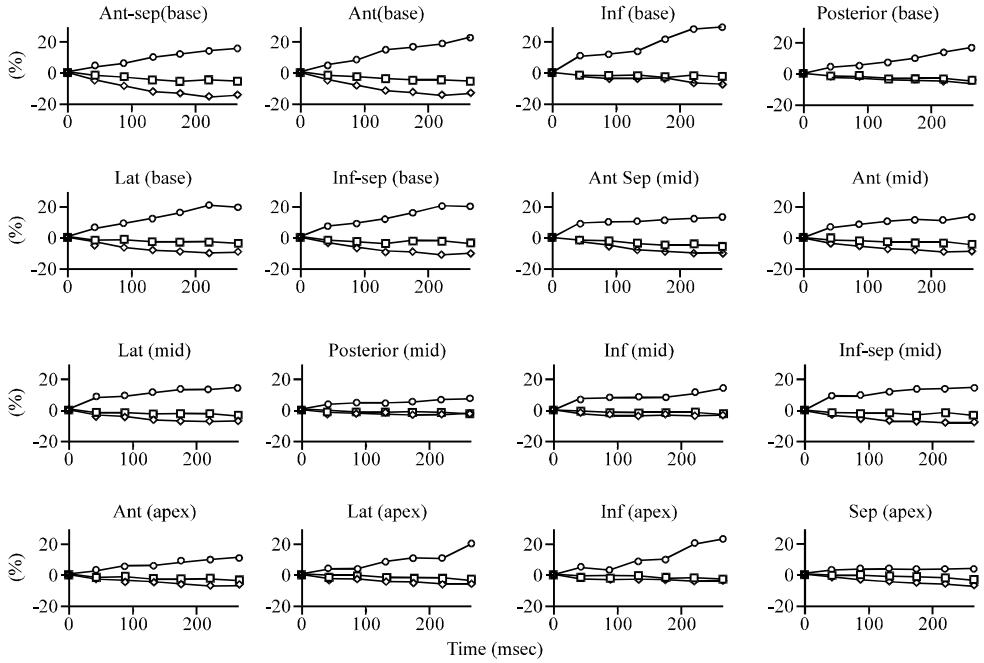

Fig. 13: Normal strain plots across a normal human data set for each of the 16 regions of LV. The different geometric shapes (circle, diamond and square), represent the radial, circumferential and longitudinal strain values, respectively

image sequences. The algorithm is capable of obtaining the strains in all points of the template. The temporal evolutions of the three axial strain components at different regions of LV from ED to ES are shown in Fig. 13. For the purpose of strain analysis, the LV was divided into three longitudinal levels (apical, mid-ventricular and basal level). The mid-ventricular and basal level was further subdivided into six sub-regions (anterior-septal, anterior, lateral, posterior, inferior-septal and septal sub-region) and four sub-regions for the apical level (septal, anterior, lateral and posterior sub-region). Mean values of the strain in these regions were calculated from the proposed model for five normal volunteer image sequences. Then, the averaging procedure is implied to these results. At all longitudinal levels and all sub-regions, the average radial, circumferential and longitudinal strains generally increased their magnitude as the cardiac cycle reached the ES. At ES, the average radial and circumferential strains reached around 0.3 and -0.15, respectively. The longitudinal strains were relatively small compared with others. These indicate that thickening of the myocardium is primarily in the radial direction and shortening is in the circumferential direction. To less extent, shortening of the myocardium is undergone in the longitudinal direction. To

evaluate the performance of algorithm, the above strain measurements were compared with previously published values (Tustison *et al*., 2003; Jinsoo and Paul, 2004) from tagged and phase contrast cardiac MRI. The average regional radial strains were well agreed with the previous studies at all longitudinal levels except for the regional radial strains in septum of apical level. In B-spline model approach (Tustison *et al*., 2003) the radial strain decreased to about -0.2 but in elastically deformable model (Jinsoo and Paul, 2004), the radial strain reached around +0.3. Our proposed value in this case is equal to 0.018. The circumferential and longitudinal strains results were the same as those obtained from others (Tustison *et al*., 2003; Jinsoo and Paul, 2004).

Interpretation of results: Average radial, circumferential and longitudinal normal strains are given in Fig. 13. The radial strains remain positive for the 16 regions indicative of the systolic thickening of LV. Both the circumferential and longitudinal strains are negative. Circumferential shortening during LV contraction results in the negative strain values in the circumferential direction while compression in the longitudinal direction results in negative longitudinal strains. These results are comparable with other relevant studys (Jinsoo and Paul, 2004; Bistoquet *et al*., 2007).

CONCLUSION

This study presented a new method for the point wise tracking of the myocardium in LV for assessing myocardial viability by reconstructing 3-D displacement fields based on 3D-AMM. It is a generalization of the original elastic model which penalizes deformations away from a preset value as opposed to simply all deformations. The novelty of the method might be the model initializing, fitting and at the conclusion of model fitting. Extraction of the dense 3D myocardial displacements and 3D myocardial strain maps are available. The advantages of the proposed method can be summarized as follows: its independency on image modality, point-wise tracking and capability of doing deformation analysis as well as its swift and robust tracking algorithm (according to Table 2). It may be used for analysis of the full 3D deformation of LV. To do this we make use of SA images of LV (CMRI). We illustrated these abilities with results from reconstruction of the deformation field within the myocardium for five normal volunteers, one patient and two synthetic data sets of image sequences. The 3D motion of LV was tracked throughout the entire cardiac cycle and a quantitative strain analysis was carried out for five normal volunteer. The results showed that the strain measurements were generally found to be consistent with mentioned published values. The results from quantitative analysis on a patient data set are consistent with the clinical evidence of the patient.

Further and future research involves the assessment and improvements of the proposed method for larger data sets. Unfortunately, we couldn't access to CMRI sequences with implanted markers for comparison between marker trajectories and trajectories which are derived from proposed algorithm. According to the ability of the proposed algorithm, we will extend performance of the algorithm with global functional analysis such as LV volume, mass and ejection fraction. It is also merged by level set segmentation procedure which was presented in FIMH2007. Some studys are in progress to make the model initialization procedure better and integrate cardiac muscle nonlinearity into our model. In addition, we are planning to combine the proposed restricted 3D block matching algorithm with other similarity measures such as shape properties which seems to be a better choice for obtaining initial displacement data and then gain access to more accurate external forces.

REFERENCES

Arts, T., W. Hunter, A. Douglas, A. Muijtjens and R. Reneman, 1992. Description of the deformation of the left ventricle by a kinematic model. J. Biomech., 25: 1119-1127.

Bardinet, E., L.D. Cohen and N. Ayache, 1996. Tracking and motion analysis of the left ventricle with deformable superquadrics. Med. Image Anal., 1: 129-149.

Benayoun, S. and N. Ayache, 1998. Dense non-rigid motion estimation in sequences of medical images using differential constraints. Int. J. Comput. Vis., 26: 25-40.

Bistoquet, A., J. Oshinski and O. Skrinjar, 2007. Left ventricular deformation recovery from cine MRI using an incompressible model. IEEE Trans. Med. Imag, 26: 1136-1153.

Denney, T.S. and J.L. Prince, 1995. Reconstruction of 3-D left ventricular motion from planar tagged cardiac MR images: An estimation theoretic approach. IEEE Trans. Med. Image, 14: 625-635.

Duncan, J.S. and A.N. Jan, 2000. Medical image analysis: Progress over two decades and the challenges ahead. IEEE Trans. Pattern Anal. Mach. Intell., 22: 85-106.

Frangi, A., W. Niessen and M. Viergever, 2001. Three-dimensional modeling for functional analysis of cardiac images: A review. IEEE Trans. Med. Imag, 20: 2-25.

Heiberg, E., L. Wigström, M. Carlsson, A.F. Bolger and M. Karlsson, 2005. Time resolved three-dimensional segmentation of the left ventricle. Proceeding of IEEE Computers in Cardiology. Sept. 25-28, Lyon, France, pp: 599-602.

Huang, J., D. Abendschein, V.G. Davila-Roman and A.A. Amini, 1999. Spatio-temporal tracking of myocardial deformations with a 4-D B-spline model from tagged MRI. IEEE Trans. Med. Image, 18: 957-972.

Jamali Dinani, F., P. Mosayebi, H. Abrishami-Moghaddam, M. Giti and S. Kermani, 2007. A fully 3D system for cardiac wall deformation analysis in MRI data. Proc. FIMH2007, 4466: 12-21.

Jinsoo, C. and J.B. Paul, 2004. Elastically deformable model based motion tracking of Left ventricle. Proceeding of 26th Annual International Conference. Sept. 1-5, IEEE, EMBS, San Francisco, CA, USA., pp: 1925-1928.

Lautissier, J., L. Legrand, A. Lalande, P. Walker and F. Brunotte, 2003. Object tracking in medical imaging using a 2D active mesh system. Proceedings of the 25th Annual International Conference of the IEEE Engineering in Medicine and Biology Society. Sept. 17-21, Cancun, Mexico, pp: 17-21.

Lötjönen, J., S. Kivistö, J. Koikkalainen, D. Smutek and K. Lauerma, 2004. Statistical shape model of atria, ventricles and epicardium from short and long-axis MR images. Med. Image Anal., 8: 371-386.

McEachen, J.C. and J.S. Duncan, 1997. Shape-based tracking of left ventricular wall motion. IEEE. Trans. Med. Image, 16: 270-283.

McInerney, T. and D. Terzopoulos, 1996. Deformable models in medical image analysis: A survey. Med. Image Anal., 1: 91-108.

Montagnat, J., H. Delingette and N. Ayache, 2001. A review of deformable surfaces: Topology, geometry and deformation. Image Vis. Comput., 19: 1023-1040.

Montagnat, J. and H. Delingette, 2005. 4D deformable models with temporal constraints: Application to 4D cardiac image segmentation. Med. Image Anal., 9: 87-100.

Moore, C.C., C.H. Lugo-Olivieri, E.R. McVeigh and E.A. Zerhouni, 2000. Three-dimensional systolic strain patterns in the normal human left ventricle: Characterization with tagged MR imaging. Radiology, 21: 453-466.

Papademetris, X., A.J. Sinusas, D.P. Dione and J.S. Duncan, 2001. Estimation of 3D left ventricular deformation from echocardiography. Med. Image Anal., 5: 17-28.

Papademetris, X., A.J. Sinusas, D.P. Dione, R.T. Constable and J.S. Duncan, 2002. Estimation of 3-D left ventricular deformation from medical images using biomechanical models. IEEE Trans. Med. Image, 21: 786-800.

Park, J., D.N. Metaxas and L. Axel, 1996. Analysis of left ventricular wall motion based on volumetric deformable models and MRI-SPAMM. Med. Image Anal., 1: 53-71.

Pham, Q.C., F. Vincent, P. Clarysse, P. Croisille and I.E. Magnin, 2001. A FEM-based deformable model for the 3D segmentation and tracking of the heart in cardiac MRI. Proceeding of the IEEE 2nd International Symposium Image and Signal Processing and Analysis (ISPA2001). June 19-21, Pula, Croatia, pp: 250-254.

Rueckert, D., A. Frangi and J. Schnabel, 2003. Automatic construction of 3-D statistical deforma- tion models of the brain using nonrigid registration. IEEE. Trans. Med. Image, 22: 1014-1025.

Shi, P., A.J. Sinusas, R.T. Constable and J. Duncan, 1999. Volumetric deformation analysis using mechanics-based data fusion: Applications in cardiac motion recovery. Int. J. Comput. Vis., 35: 87-107.

Shi, P., A.J. Sinusas, R.T. Constable, E. Ritman and J.S. Duncan, 2000. Point-tracked quantitative analysis of left ventricular surface motion from 3-D image sequences. IEEE Trans. Med. Image, 19: 36-50.

Si, H., 2006. On refinement of constrained delaunay tetrahedralizations. Proceedings 15th International Meshing Roundtable. September 17-20, Springer-Verlag, pp: 509-528.

Tirupathi, R., R. Chandrupatla and A.D. Belegundu, 2002. Introduction to Finite Elements in Engineering. 3rd Edn., Prentice-Hall Inc., ISBN: 0132070367.

Tustison, N.J., V.G. Dávila-Román and A.A. Amini, 2003. Myocardial kinematics from tagged MRI based on a 4-D B-spline model. IEEE Trans. Biomedical Eng., 50: 1038-1040.

Young, A.A., D.L. Kraitchman, L. Dougherty and L. Axel, 1995. Tracking and finite element analysis of stripe deformation in magnetic resonance tagging. IEEE Trans. Med. Image, 14: 413-421.